Assessment of Subsynchronous Oscillations in AC grid-connected VSC Systems with Type-4 Wind Turbines

Luis Sainz[1*], Lluis Monjo[2], Marc Cheah-Mane[3], J. Liang[4]

[1] Department of Electrical Engineering, ETSEIB-UPC, Av. Diagonal 647, 08028 Barcelona, Spain
[2] Department of Industrial and Design System Engeneering, Univ. Jaume I, Av. de Vicent Sos Baynat, s/n, 12071 Castelló de la Plana, Spain
[3] Department of Electrical Engineering, CITCEA-UPC, Av. Diagonal 647, 08028 Barcelona, Spain
[4] School of Engineering, Cardiff University, CF24 3AA, Cardiff, U.K
[*] sainz@ee.upc.edu

Abstract: Converters are the key for the increasing development of renewable energy generation but their dynamic interaction with the grid has an important impact on stability. Oscillatory instabilities in different grid-connected converter systems at several frequency ranges are reported. In particular, sub and supersynchronous oscillatory instabilities in AC power systems with type-3 and type-4 wind turbine generators were recently registered at several wind farm areas. A number of works based on eigenvalue analysis and frequency domain approaches are carried out to analyze this new stability issue and more research is going on to analyze in detail the electric and control parameters that may affect this phenomenon. This paper contributes analyzing in detail the influence of system parameters on the subsynchronous oscillations in AC power systems with type-4 wind turbine generators. This study is based on a new approach for subsynchronous stability assessment which could also be used for analyzing other types of subsynchronous oscillations (e.g., subsynchronous control interactions between doubly-fed induction generators and series-compensated networks) as well as supersynchronous oscillations. A representative example of weak AC grids with type-4 wind turbine generators is used to illustrate the contributions of the paper. Results are validated with PSCAD/EMTDC time-domain simulations.

Nomenclature

AC	Alternating current
CC	Current controller
DC	Direct current
DFIG	Doubly-fed induction generator
DFT	Direct Fourier Transform
DVC	DC-link voltage controller
EMTDC	Electromagnetic transient design and control
GNC	General Nyquist criterion
HVDC	High voltage direct current
PI	Proportional-integral
PLL	Phase-locked loop
PMSG	Permanent magnet synchronous generator
PSCAD	Power Systems Computer Aided Design
PSS	Power System Stabilizers
SSO	Subsynchronous oscillation
WPP	Wind power plant
WTG	Wind turbine generator
VSC	Voltage source converter
SCR	Short-circuit ratio

1. Introduction

Renewables are currently become a clean source of energy in power systems. In particular, the presence of solar and wind power plants (WPPs) is increasing all over the world [1], [2]. These plants are usually aggregated in large solar and wind energy areas far away from demand centers. High-voltage DC (HVDC) is currently the rising transmission system for delivering all power of these solar and wind energy areas through long-distance lines while AC grids are commonly used to interconnect the different renewable energy plants (and also power and thermal power plants) inside these areas [1], [3]. Wind turbine generators (WTGs) based on partial-scale power converters (type-3 WTGs) [4] – [6] and fully-rated power converters (type-4 WTGs) [7] are mainly used in WPPs. Power electronic converters such as voltage source converters (VSCs) are used to connect WTGs with power systems playing an important role for the development of renewable energy generation. However, they also bring new challenges and problems due to their differences with traditional power system components such as synchronous generators, transformers and lines [1]. One of the most important problems is the interactions between the WTG control and grids which may lead to oscillatory instabilities. These instabilities are classified in two categories depending on their frequency range [1], [8]: (i) Harmonic oscillations which approximately range from 0.1 to 2 kHz. (ii) Near-synchronous oscillations which can be divided in subsynchronous oscillations (SSOs) and super-synchronous oscillations approximately ranging from 15 to 45 Hz and 55 to 100 Hz, respectively. Harmonic oscillatory instabilities are well-documented and studied phenomena in several VSC applications such as HVDC links [9], wind power plants [10] and ac traction systems [11]. Subsynchronous [1], [3], [6], [12], [13] and supersynchronous [1] oscillatory instabilities are new reported phenomena in power systems which are currently being studied. In particular, SSOs caused by the interactions between doubly-fed induction generators (DFIGs) and fixed series compensators were observed in Texas (USA) [14] and Guyuan area, Hebei Province (North-China) [6], [12]. Currently,

subsynchronous [1], [3], [13] and supersynchronous [1] oscillations caused by the interactions between type-4 WTGs and AC weak grids were observed in Hami area, Xinjiang province (North-China). In traditional power systems, damping of resistive loads is sufficient to prevent these instabilities but they may arise in systems with large penetration of grid-connected VSCs, where resistive and rotating mass loads are limited. It is common for low-frequency electro-mechanical oscillations to appear due to low damping. These oscillations are usually avoided by means of power system stabilizers (PSSs) [15] – [17]. Such controllers are also applied in grid-connected VSCs to introduce active damping [18], [19].

There are several studies about SSOs between type-4 WTGs and AC grids [3], [13], [20] – [24]. Preliminary studies in [23], [24] point out that there is no impact of type-4 WTGs on SSOs. Nevertheless, more recent studies in [20] – [22] focused on frequency response of VSC input admittance and they show that VSCs may introduce negative damping in the grid at near-synchronous frequencies that could cause SSOs. This is confirmed by actual observations newly presented in [3], [13]. Traditional stability criteria such as state space eigenvalue analysis and generalized Nyquist criterion (GNC) are commonly used for examining this phenomenon [3], [6], [8], [9], [20] – [22], [25], [26]. State space eigenvalue analysis requires detailed information for all elements in the system which is not always completely available. On the other hand, frequency domain methods as GNC can be applied by using system measurements if the parameter information is not available [13], [26]. The GNC only provides qualitative results because it focuses on the matrix transfer function of the entire system which does not allow investigating separately the contribution of the grid and VSCs to the closed-loop stability [3]. Also, sequence impedance model based analysis is recently used to assess the contribution of the system parameters to SSOs [1], but it may provide inaccurate stability predictions [27]. A criterion based on the impedance matrix determinant characteristics of the system impedance matrix is recently proposed in [3] to overcome the drawbacks of the previous approaches. However, this criterion focuses on the impedance matrix determinant of the entire system which limits to investigate separately the influence of the grid and VSCs on stability.

This paper investigates the influence of system parameters on SSOs between type-4 WTGs and AC grids by using a new developed approach based on the impedance matrix determinant-based stability criterion in [3]. This approach shows the contribution that grid and VSC have on stability. A representative system of weak grids with type-4 WTGs is analyzed to show the contributions of the paper. Several conclusions about the influence that converter control and grid parameters have on stability are reported analyzing the interaction of the grid and VSC. Results are validated with time-domain simulations in PSCAD/EMTDC.

The rest of the paper is organized as follows: Section 2 presents grid-connected VSC modelling for stability studies. Section 3 reviews the criteria for SSO analysis of grid-connected VSCs. Section 4 deals with the study of the new alternative approach to assessing SSOs. A PSCAD/EMTDC application is presented in Section 5 to validate the study. Conclusions are drawn in Section 6.

2. Grid-connected VSC modelling

The influence of type-4 WTGs on subsynchronous instabilities mainly depends on the dynamics of the VSCs connecting WTG with the grid. Such instabilities can be investigated in frequency-domain using the *dq*-frame impedance-based representation of the grid-connected VSCs in Fig. 1 [3], [20] – [22]. Capacitor filter at VSC terminal is omitted because it does not affect significantly SSOs.

2.1. VSC model

According to Fig. 1, the VSC control is represented with the inner current controller (CC) and the outer DC-link voltage controller (DVC) as well as the phase-locked loop (PLL). The DVC generates the *d*-component of the CC reference current i_{dref} and the PLL drives the *q*-component of the voltage *v* in the converter *dq*-frame to zero providing the transformation angle θ. The *q*-component of the CC reference current i_{qref} is set to zero by assuming that VSC is operating at unity power factor which is common in normal operation conditions [3], [20], [22].

The small-signal model of the VSC is derived and well-documented in [20] – [22] as

$$Z_{vsc}(s)=\frac{\Delta v}{\Delta i}=\begin{bmatrix} Z_{v,dd}(s) & 0 \\ 0 & Z_{v,qq}(s) \end{bmatrix}$$
$$Z_{v,dd}(s)=\left(y_{cc}(s)-g_{cc}(s)G_{dc}(s)\right)^{-1} \quad (1)$$
$$Z_{v,qq}(s)=\left(y_{cc}(s)\left(1-v_0G_{PLL}(s)\right)+\left\{P_0/v_0\right\}G_{PLL}(s)\right)^{-1},$$

where

- The variables $v=[v_d\ v_q]^{\mathrm{T}}$ and $i=[i_d\ i_q]^{\mathrm{T}}$ are the real

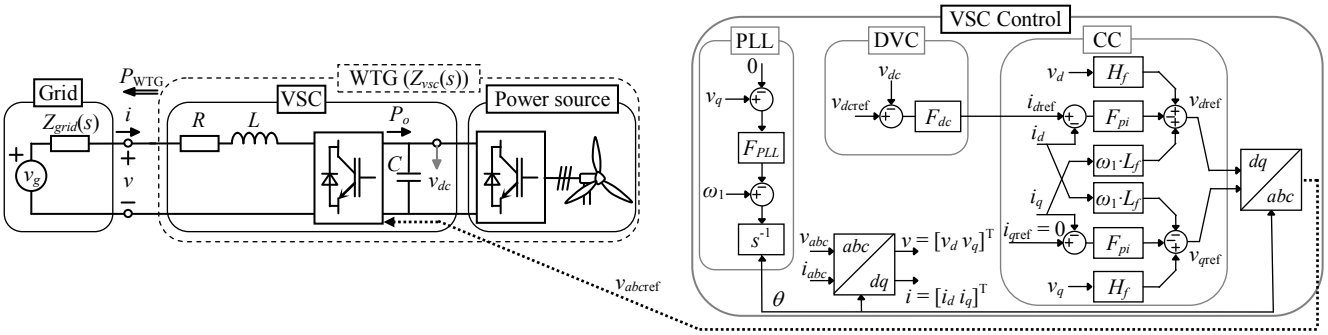

Fig. 1. *Grid-connected VSC system model*

space vectors of the VSC input voltage and current in *dq*-frame.

- The transfer functions $g_{cc}(s)$ and $y_{cc}(s)$ characterize the CC dynamics,

$$g_{cc}(s)=\frac{k_p s+k_i}{Ls^2+(R+k_p)s+k_i}$$
$$y_{cc}(s)=\frac{s^2}{Ls^3+(L\omega_f+k_p)s^2+(R+k_p\omega_f+k_i)s+k_i\omega_f}, \quad (2)$$

where R and L are the resistance and inductance of the VSC filter, $k_p = \omega_c \cdot L$ and $k_i = \omega_c \cdot R$ are the gains of the proportional-integral (PI) CC $F_{pi}(s) = k_p + k_i/s$, $\omega_c \le 0.2 \cdot (2\pi f_{sw})$ is the bandwidth of the inner current control loop, f_{sw} is the VSC switching frequency and $\omega_f \le 0.1 \cdot \omega_c$ is the bandwidth of the feed-forward voltage low-pass filter $H_f(s) = \omega_f/(s + \omega_f)$ [22].

- The transfer function $G_{dc}(s)$ characterizes the dynamics of the reference current i_{dref} due to change in the VSC input voltage v by considering the outer loop of the DVC,

$$G_{dc}(s)=\frac{F_{dc}(s)\left[v_0^2 y_{cc}(s)+P_0\right]}{v_0^2(Cs+g_{cc}(s)F_{dc}(s))}, \quad (3)$$

where C is the DC capacitance and $F_{dc}(s) = k_{p\text{-}dc} + k_{i\text{-}dc}/s$ is the PI DVC, $k_{p\text{-}dc} = \omega_{dc}C$ and $\omega_{dc} \le 0.1 \cdot \omega_c$ is the bandwidth of the outer DC-link voltage control loop [20], [23].

- The transfer function $G_{PLL}(s)$ characterizes the dynamics of the PLL,

$$G_{PLL}(s)=\frac{F_{PLL}(s)}{s+v_0 F_{PLL}(s)}, \quad (4)$$

where $F_{PLL}(s) = k_{p\text{-}PLL} + k_{i\text{-}PLL}/s$ is the PI controller of the PLL, $k_{p\text{-}PLL} = \omega_p/v_0$ and $\omega_p \le 0.1 \cdot \omega_c$ is the bandwidth of the PLL control loop [22].

- The variables v_0 and P_0 are the steady-state operation points of VSC input voltage and DC output power (see Fig. 1).
- The off-diagonal elements of $Z_{vsc}(s)$ are zero because reactive power or AC voltage controls are not considered. This is a usual procedure for approximately analyzing the effects of CC, DVC and PLL on stability [3], [20] – [22].

2.2. Grid model

The dynamic equations of the grid in *dq*-frame with the VSC input voltage v and current i are

$$v_g=\begin{bmatrix} v_{gd} \\ v_{gq} \end{bmatrix}=\underbrace{\begin{bmatrix} Z_{g,dd}(s) & Z_{g,dq}(s) \\ Z_{g,qd}(s) & Z_{g,qq}(s) \end{bmatrix}}_{Z_{grid}(s)} i+v. \quad (5)$$

For symmetric systems, the relations $Z_{g,dd}(s) = Z_{g,qq}(s)$ and $Z_{g,dq}(s) = -Z_{g,qd}(s)$ hold. In particular, transformers and medium and high voltage lines can be modeled as R-L circuits at subsynchronous frequencies (equivalent shunt capacitors are neglected in line models) and the impedance matrix of these components is [25]

$$Z_{comp}(s)=\begin{bmatrix} R_g+L_g s & -L_g\omega_1 \\ L_g\omega_1 & R+L_g s \end{bmatrix}, \quad (6)$$

where $\omega_1 = 2\pi f_1$ ($f_1 = 50$ Hz) is the fundamental angular frequency of the grid. The impedance matrix of the grid commonly presents the same structure as $Z_{comp}(s)$ [3], [25].

2.3. Grid-connected VSC model

The impedance-based equivalent circuit of the grid-connected VSC system is obtained by replacing the WTG in Fig. 1 with $Z_{vsc}(s)$ (1) and characterizing the grid as the voltage source v_g in series with the equivalent impedance matrix $Z_{grid}(s)$ (5). The small-signal dynamics of the grid-connected VSC system can be analyzed from the expression:

$$\Delta i=\underbrace{\left(Z_{vsc}(s)+Z_{grid}(s)\right)^{-1}}_{Y_{sys}(s)=Z_{sys}^{-1}(s)}\Delta v$$
$$=(1+\underbrace{Z_{vsc}^{-1}(s)Z_{grid}(s)}_{L(s)})^{-1}Z_{vsc}^{-1}(s)\Delta v. \quad (7)$$

It must be highlighted that, although the off-diagonal elements of $Z_{vsc}(s)$ are zero, coupling between *d*- and *q*-axis components are identified on the grid-connected VSC impedance in (7) due to the grid impedance.

3. Stability analysis of grid-connected VSC systems

Near-synchronous oscillatory instabilities are mainly due to the outer control and grid synchronization loop (designed with lower bandwidths than the CC loop) [20] – [22], and they must be studied in frequency domain from the system matrix impedance modelling (7) due to the asymmetries introduced in the VSC model by these loops [25]. This makes difficult to analyze the contribution of the VSC and grid to the oscillations. In this case, stability of grid-connected VSC systems is usually assessed by either determining the poles of the closed-loop system $Y_{sys}(s)$ (i.e., the state-space eigenvalues of the system) or applying the GNC to the open-loop transfer matrix $L(s) = Z^{-1}{}_{vsc}(s)Z_{grid}(s) = Y_{vsc}(s)Z_{grid}(s)$ [25]. The state space eigenvalue analysis is a useful tool to analyze the impact of system and control parameters on stability. However, this method requires detailed information for the physical and control parameters in the system and high-order dynamic models for large systems [13], [26]. The GNC extends the traditional Nyquist criterion to the Nyquist curves of the eigenvalues of $L(s)$ [25], i.e.

$$\det\left[\lambda_i(s)I-L(s)\right]=0 \qquad (i=1,2) \quad \Rightarrow \quad \lambda_{1,2}(s)=$$
$$\frac{L_{dd}(s)+L_{qq}(s)}{2}\pm\sqrt{\left(\frac{L_{dd}(s)-L_{qq}(s)}{2}\right)^2+L_{dq}(s)L_{qd}(s)}. \quad (8)$$

Although GNC is commonly used, it only shows numerical results because it focuses on the open-loop transfer function of the entire system which does not allow investigating separately the contribution of the grid and VSCs to the closed-loop stability [3]. Sequence impedance analysis is also used to assess the contribution of the system parameters to SSOs from two independent single-input-single-output systems [1], but this method may lead to inaccurate stability predictions because the coupling between the sequence components is neglected [24].

To address the issues of the above approaches, [3] proposes the impedance matrix determinant-based stability criterion based on the frequency domain representation of the determinant of $Z_{sys}(s)$, $D(s) = \det[Z_{sys}(s)]$. The admittance matrix in (7) can be expressed as

$$Y_{sys}(s) = Z_{sys}^{-1}(s) = \frac{1}{D(s)}\mathrm{adj}\left[Z_{sys}(s)\right], \tag{9}$$

where $\mathrm{adj}[Z_{sys}(s)]$ denotes the adjoint of $Z_{sys}(s)$. According to (9), the poles of the closed-loop system $Y_{sys}(s)$ can also be obtained from the zeros of $D(s)$ [3]. Considering the difficulty to determine the zeros of $D(s)$ in actual systems due to its high order, the impedance matrix determinant-based stability criterion assesses the oscillatory stability of the poorly damped zeros of $D(s)$ by analyzing its frequency domain plot [3]. If $z_o = \sigma_o \pm j\omega_o$ are a pair of conjugate zeros of $D(s)$, the frequency domain representation of $D(s)$ can be expressed as follows [12], [13]:

$$D(j\omega) = (j\omega - z_o)(j\omega - z_o^*)H(j\omega), \tag{10}$$

which can be approximated in a small neighbourhood of ω_o as

$$\begin{aligned} &D(j\omega) \approx (\sigma_o^2 + \omega_o^2 - \omega^2 - j2\omega\sigma_o)H(j\omega_o) = \\ &\underbrace{H_r(\sigma_o^2 + \omega_o^2 - \omega^2) + 2H_x\omega\sigma_o}_{D_r(\omega)} + j\underbrace{(H_x(\sigma_o^2 + \omega_o^2 - \omega^2) - 2H_r\omega\sigma_o)}_{D_x(\omega)}, \end{aligned} \tag{11}$$

by assuming that $[H(j\omega)]_{\omega \approx \omega o} \approx H_r + jH_x$ with H_r and H_x constant values. The zero-crossing frequency of the imaginary part of $D(j\omega)|$ is only analyzed in [3], [12], [13] by solving $D_x(\omega) = 0$. The present paper further analyses (11) and it determines the zero-crossing frequencies ω_r and ω_x of the real and imaginary parts of $D(j\omega)|$ by solving $D_r(\omega) = 0$ and $D_x(\omega) = 0$, respectively,

$$\begin{aligned} \omega_r &= \frac{H_x}{H_r}\sigma_o \pm \sqrt{\left(\frac{H_x}{H_r}\sigma_o\right)^2 + (\sigma_0^2 + \omega_o^2)} \\ \omega_x &= -\frac{H_r}{H_x}\sigma_o \pm \sqrt{\left(\frac{H_r}{H_x}\sigma_o\right)^2 + (\sigma_0^2 + \omega_o^2)}, \end{aligned} \tag{12}$$

where the feasible solutions correspond to positive zero-crossing frequency values with the largest magnitude.

The frequency of oscillation modes related to poorly damped zeros are obtained from the zero-crossing frequencies in (12). In case of poorly damped zeros, such zeros have $|\sigma_o| << |\omega_o|$, which implies that ω_r and ω_x are very close and approximately match with the frequency of oscillatory modes, i.e. $\omega_r \approx \omega_x \approx \omega_o$. The zero-crossing frequency that best approximates the subsynchronous oscillation frequency ω_o depends on the ratio between H_r and H_x: If $H_r < H_x$, $\omega_o \approx \omega_x$, otherwise $\omega_o \approx \omega_r$. Subsequently, the subsynchronous oscillation stability, characterized by the sign of σ_o, is assessed from the real or imaginary part of $D(j\omega)$ depending on the ratio between H_r and H_x and considering the poorly damped zero assumption $|\sigma_o| << |\omega_o|$:

- If $H_r < H_x$, the real part of $D(j\omega)$ at ω_x is approximated as

$$D_r(\omega_x) \approx -k_x\sigma_o, \tag{13}$$

where k_x is the slope of $D_x(\omega)$ at ω_x, i.e,

$$k_x = \left[\frac{dD_x(\omega)}{d\omega}\right]_{\omega=\omega_x} \approx -2H_x\omega_x. \tag{14}$$

Therefore, the subsynchronous oscillation is stable (i.e., $\sigma_o < 0$) when

$$D_r(\omega_x) > 0 \text{ if } k_x > 0 \quad \text{or} \quad D_r(\omega_x) < 0 \text{ if } k_x < 0. \tag{15}$$

- If $H_r > H_x$, the imaginary part of $D(j\omega)$ at ω_r is approximated as

$$D_x(\omega_r) \approx k_r\sigma_o, \tag{16}$$

where k_r is the slope of $D_r(\omega)$ at ω_r, i.e,

$$k_r = \left[\frac{dD_r(\omega)}{d\omega}\right]_{\omega=\omega_r} \approx -2H_r\omega_r. \tag{17}$$

Therefore, the subsynchronous oscillation is stable (i.e., $\sigma_o < 0$) when

$$D_x(\omega_r) < 0 \text{ if } k_r > 0 \quad \text{or} \quad D_x(\omega_r) > 0 \text{ if } k_r < 0. \tag{18}$$

According to the Appendix, it can be concluded that the result of the stability study does not depend on the ratio between H_r and H_x, i.e., both criteria (15) and (18) can be applied for stability assessment independently of the ratio between H_r and H_x. The real part zero-crossing frequency criterion (18) is a novel alternative to the imaginary part zero-crossing frequency criterion (15).

The impedance matrix determinant-based stability criterion is a practical approach to address subsynchronous oscillation concerns because it allows easily quantifying the oscillatory stability by observing the frequency plots (real and imaginary parts) of the determinant of the system impedance matrix. However, the determinant only focuses on the frequency response of the entire system which does not allow investigating separately the contribution of the grid and VSC to the closed-loop stability. This limits the

analysis of oscillations caused by particular impedances of the grid or filters connected to the system as well as VSC control parameters. This drawback is avoided in next Section by analyzing the terms of the system impedance matrix $Z_{sys}(s)$.

4. Alternative approach to assess SSOs

According to (1) and (5), the frequency response of the system impedance matrix is obtained by setting $s = j\omega$ in (7) and can be expressed as follows

$$\begin{aligned} &Z_{sys}(j\omega) = \\ &\begin{bmatrix} Z_{v,dd}(j\omega) & 0 \\ 0 & Z_{v,qq}(j\omega) \end{bmatrix} + \begin{bmatrix} Z_{g,dd}(j\omega) & Z_{g,dq}(j\omega) \\ Z_{g,qd}(j\omega) & Z_{g,qq}(j\omega) \end{bmatrix} \\ &= \begin{bmatrix} R_{dd}+jX_{dd} & R_{g,dq}+jX_{g,dq} \\ R_{g,qd}+jX_{g,qd} & R_{qq}+jX_{qq} \end{bmatrix} \end{aligned} \tag{19}$$

$$R_{ii}+jX_{ii} = R_{v,ii}+R_{g,ii}+j(X_{v,ii}+X_{g,ii}) \qquad (ii = dd, qq),$$

and the real and imaginary parts of its determinant can be written as

$$\begin{aligned} D(j\omega) &= \underbrace{R_{dd}R_{qq} - X_{dd}X_{qq} - (R_{g,dq}R_{g,qd} - X_{g,dq}X_{g,qd})}_{D_r(\omega)} \\ &+ j(\underbrace{R_{dd}X_{qq} + R_{qq}X_{dd} - (R_{g,dq}X_{g,qd} + R_{g,qd}X_{g,dq})}_{D_x(\omega)}), \end{aligned} \tag{20}$$

where the resistances and reactances functions $R(\omega)$ and $X(\omega)$ are expressed as R and X to simplify the notation.

Considering (20) and the stability criterion in [3] (see Section 3), the closed-loop stability can be assessed as follows,

- If $H_r < H_x$, the subsynchronous oscillation is stable (15) if one of the following conditions are verified at ω_x

$$\begin{aligned} &\overbrace{R_{dd}R_{qq} - X_{dd}X_{qq}}^{D_{r,vsc}(\omega_x)} > \overbrace{R_{g,dq}R_{g,qd} - X_{g,dq}X_{g,qd}}^{D_{r,grid}(\omega_x)} \quad (k_x > 0) \\ &R_{dd}R_{qq} - X_{dd}X_{qq} < R_{g,dq}R_{g,qd} - X_{g,dq}X_{g,qd} \quad (k_x < 0). \end{aligned} \tag{26}$$

- If $H_r > H_x$, the subsynchronous oscillation is stable (18) if one of the following conditions are verified at ω_r

$$\begin{aligned} &\overbrace{R_{dd}X_{qq} + R_{qq}X_{dd}}^{D_{x,vsc}(\omega_r)} < \overbrace{R_{g,dq}X_{g,qd} + R_{g,qd}X_{g,dq}}^{D_{x,grid}(\omega_r)} \quad (k_r > 0) \\ &R_{dd}X_{qq} + R_{qq}X_{dd} > R_{g,dq}X_{g,qd} + R_{g,qd}X_{g,dq} \quad (k_r < 0). \end{aligned} \tag{22}$$

It must be noted that the right terms of the inequalities, $D_{r,grid}(\omega_x)$ and $D_{x,grid}(\omega_r)$, only depend on the grid and they are called as grid terms. On the other hand, the left terms, $D_{r,vsc}(\omega_x)$ and $D_{x,vsc}(\omega_r)$, are called as VSC terms because it is numerically verified that they are mainly affected by the VSC. This is because the contribution of the grid reactances at subsynchronous frequencies, $X_{g,dd} = X_{g,qq} = L_g\omega$ ($\omega < \omega_1$), is smaller than the contribution of the grid reactances at synchronous frequency, $X_{g,dq} = X_{g,qd} = L_g\omega_1$ (see Section 5). Therefore, the contribution of the grid and VSC subsystems to the closed-loop stability can be approximately analyzed from the comparison of the frequency response of the grid and VSC terms of the inequalities (21) or (22).

Considering (6), the frequency response of transmission grids ($R_g < L_g\omega$) at subsynchronous frequencies may usually be approximated as

$$\begin{aligned} &Z_{grid}(j\omega) \approx \\ &\begin{bmatrix} R_g + jL_g\omega & -L_g\omega_1 \\ L_g\omega_1 & R_g + jL_g\omega \end{bmatrix} \approx \begin{bmatrix} jL_g\omega & -L_g\omega_1 \\ L_g\omega_1 & jL_g\omega \end{bmatrix}, \end{aligned} \tag{23}$$

and the inequalities (21) or (22) become,

- If $H_r < H_x$, the subsynchronous oscillation is stable if one of the following conditions are verified at ω_x

$$\begin{aligned} &\overbrace{R_{v,dd}R_{v,qq} - (X_{v,dd}+X_g)(X_{v,qq}+X_g)}^{D_{r,vsc}(\omega_x)} > \overbrace{-X_{g1}^2}^{D_{r,grid}(\omega_x)} \quad (k_x > 0) \\ &R_{v,dd}R_{v,qq} - (X_{v,dd}+X_g)(X_{v,qq}+X_g) < -X_{g1}^2 \quad (k_x < 0). \end{aligned} \tag{24}$$

- If $H_r > H_x$, the subsynchronous oscillation is stable if one of the following conditions are verified at ω_r

$$\begin{aligned} &\overbrace{R_{v,dd}(X_{v,qq}+X_g) + R_{v,qq}(X_{v,dd}+X_g)}^{D_{x,vsc}(\omega_r)} < 0 \quad (k_r > 0) \\ &R_{v,dd}(X_{v,qq}+X_g) + R_{v,qq}(X_{v,dd}+X_g) > 0 \quad (k_r < 0), \end{aligned} \tag{25}$$

where $X_g = L_g\omega$ and $X_{g1} = L_g\omega_1$.

5. Application

An example of WPPs far away from consumptions as well as connected through weak AC grids proposed in [3] is analyzed. The example has a WPP with $N = 700$ identical PMSG type-4 WTGs of rated power $P_{WTG,\,\text{rated}} = 1.5$ MW connected through a local and a long-distance transmissions to the main grid (see Fig. 2). It is assumed that the WTGs operate under a similar operating point supplying an output active power $P_{\text{WTG}} \approx -P_O$ (see Fig. 1) and the possible turbine generators connected to the main grid are shut down, which are actual conditions of the detected SSOs [3]. The data of the electrical installation and the WTG VSCs are shown in [3] and Table 1, respectively. The electrical parameters of the AC grid in [3] are expressed in pu with $S_B = 1500$ MVA. WTGs operate with a low output active power P_{WTG} and the AC grid has a low value of the short-circuit ratio *SCR* equal to 1.34,

$$SCR = \frac{S_B / x_\Sigma}{N \cdot P_{WTG,\,\text{rated}}} \qquad x_\Sigma = x_{L1} + x_{L2} + x_{T2} + x_{T3}, \tag{26}$$

which corresponds to the SSO scenario observed in the actual installation in [3]. The transfer function of the system impedance matrix (7) can be derived from (1) and (6) as,

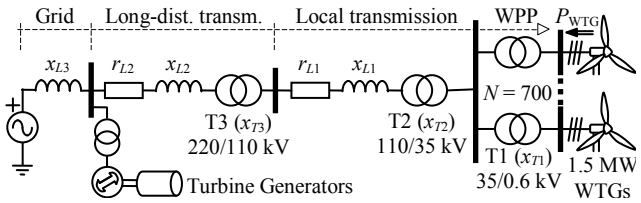

Fig. 2. *Long-distance transmission AC grid with PMSG WPPs.*

Table 1 1.5 MW WTG Parameters (50-Hz base frequency) [20], [21], [22]

	Parameters	Values
VSC input voltage	v_o (pu)	1
WTG output active power	P_{WTG} (pu)	0.1
Output L-filter	R, L (pu)	0.015, 0.15
DC Capacitance	C (pu)	13
Current controller (CC) ($k_p = \omega_c L$ $k_i = \omega_c R$)	f_{sw} (pu)	40
	$\omega_{c,\,ref}$ (pu)	3.4
	$\omega_{f,\,ref}$ (pu)	0.34
DC-link voltage controller (DVC) ($k_{p\text{-}dc} = \omega_{dc} C$ $k_{i\text{-}dc} = k_{p\text{-}dc}/25$)	$\omega_{dc,\,ref}$ (pu)	0.68
Phase-locked loop (PLL) ($k_{p\text{-}PLL} = \omega_p/v_o$ $k_{i\text{-}PLL} = k_{p\text{-}PLL}/10$)	$\omega_{p,\,ref}$ (pu)	0.25

$$Z_{sys}(s) = \begin{bmatrix} Z_{v,dd}(s)/N + Z_g(s) & -X_{g1} \\ X_{g1} & Z_{v,qq}(s)/N + Z_g(s) \end{bmatrix} \quad (27)$$

$$Z_g(s) = r_{L1} + r_{L2} + \frac{s}{\omega_1} X_{g1} \qquad X_{g1} = x_\Sigma + \frac{x_{T1}}{N},$$

and the impedance matrix (19) is obtained by setting $s = j\omega$.

Starting from an unstable reference case corresponding to the data in [3] and Table 1, the influence of system parameters on SSOs is analyzed in several cases to improve system stability. These parameters are classified in electrical (e.g., grid components) and control parameters. The latter is divided in the CC parameters and outer loop (DVC and PLL) control parameters because they have different time constants, and therefore their influence on stability may be different. Stability is assessed from the poles of the closed-loop system, the impedance matrix determinant-based stability criterion [3], the alternative approach proposed in the paper (Section 4) and the GNC (8). The study is also validated from PSCAD/EMTDC time-domain simulations.

5.1. Reference case (data in [3] and Table 1)

The system has a pair of poorly damped conjugate poles, $z_o = 11.8 \pm j(2\pi \cdot 17.8)$, with their frequencies located in the subsynchronous range and positive real parts meaning that the SSOs at these frequencies are unstable. System instability is analyzed in Fig. 3. The impedance matrix determinant-based stability criterion (15) predicts the instability because, in the neighborhood of the previous poorly damped poles, the slope of $D_x(\omega_x)$ is negative, $k_x < 0$, and $D_r(\omega_x)$ is positive, $D_r(\omega_x) > 0$, at the zero-crossing frequency of $D_x(\omega)$ $f_x = 19.3$ Hz (see in Fig. 3(a)). Note that the above frequency approximates the subsynchronous oscillation frequency of the unstable poles. According to Fig. 3(b), the alternative approach in Section 4 also confirms the instability due to $D_{r,\,vsc}(\omega_x) > D_{r,\,grid}(\omega_x) = -X_{g1}{}^2$ (24) at the zero-crossing frequencies of $D_x(\omega)$. This approach shows that the contribution of the VSC, represented by $D_{r,\,vsc}(\omega_x)$, does not compensate the large contribution of a weak grid, represented by $D_{r,\,grid}(\omega_x)$. The GNC verifies the instability results because the curve of the eigenvalue λ_2 (8) encircles the –1 point in clockwise direction (Fig. 3(c)). It is observed that the paper approach shows the individual contribution that the grid and the VSC have on the stability, while this is not possible by the impedance matrix determinant-based stability criterion and GNC. The system dynamics are investigated in Fig. 3(d) from PSCAD/EMTDC time-domain simulations in order to validate the previous stability results. The WTG output active power P_{WTG} is raised from zero to the value of the reference case ($P_{WTG} = 0.1$ pu in Table 1) at 1 s. Note that the VSC input voltage (v_d and v_q) becomes unstable after the step rise of the WTG output active power. Discrete-Fourier-transformation (DFT) of the VSC input voltage is also shown in Fig. 3(d) to illustrate the frequency of subsynchronous (≈ 17 Hz) oscillations which approximately matches with the predictions of the stability study. These SSOs in the *dq*-frame are reflected in the phase voltage and current magnitudes as subsynchronous (≈ 50 – 17 = 33 Hz) and supersynchronous (≈ 50 + 17 = 67 Hz) oscillations around the fundamental frequency which produce active power subsynchronous fluctuations at 17 Hz [1], [3]. It is worth noting that this oscillatory instability is a new phenomenon different from the classical voltage

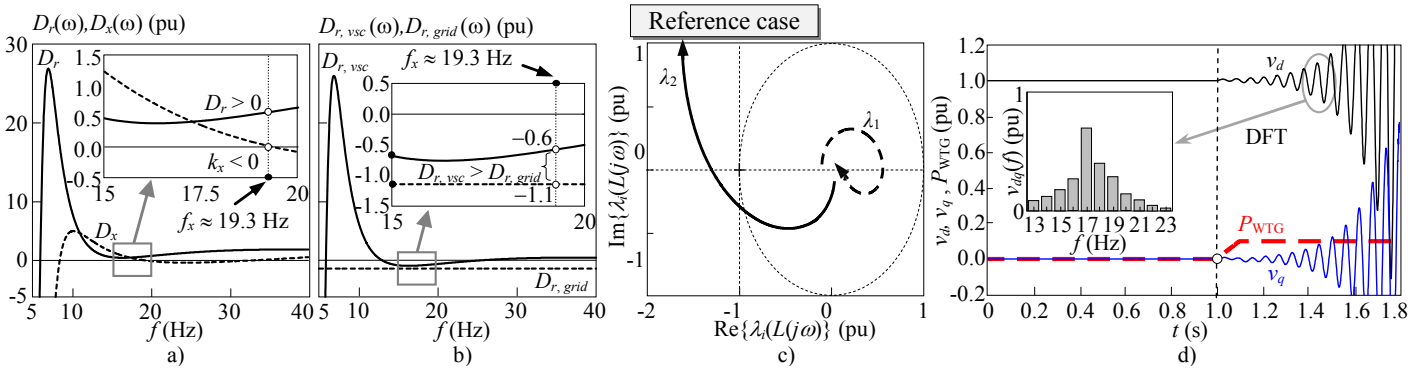

Fig. 3. *Stability study of the reference case (data in [3] and Table 1)*
(a) Impedance matrix determinant-based stability criterion, **(b)** Alternative approach, **(c)** Generalized Nyquist criterion, **(d)** PSCAD/EMTDC time-domain simulations.

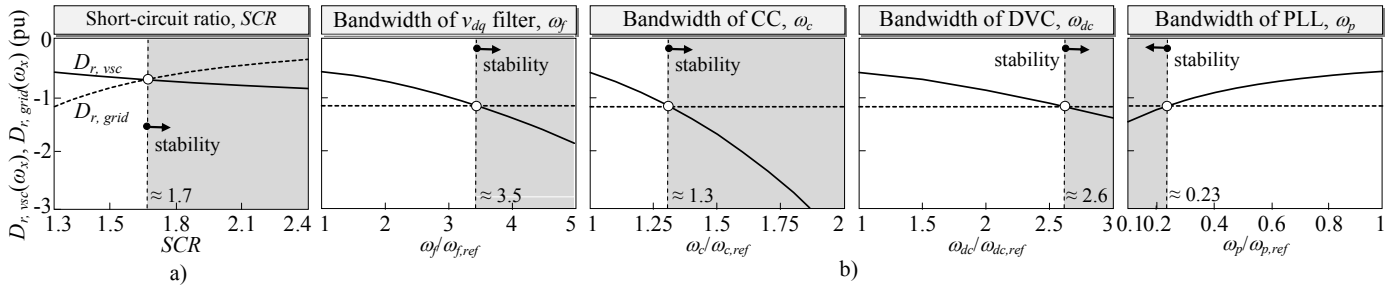

Fig. 4. *Sensitivity analysis of system parameters*
(a) *SCR*, **(b)** ω_f, ω_c, ω_{dc} and ω_p

instability due to voltage drops in weak grids [26].

5.2. Influence of electrical and control parameters

A sensitivity analysis of the impact of the main electrical and control parameters on stability is performed from the proposed approach in Fig. 4. These parameters are the short-circuit ratio, *SCR*, and control bandwidths (i.e., the bandwidths of the feed-forward voltage low-pass filter, ω_f, inner current control loop, ω_c, outer DC-link voltage control loop, ω_{dc}, and PLL control loop, ω_p). The $D_{r,\,grid}(\omega_x)$ and $D_{r,\,vsc}(\omega_x)$ values at the zero-crossing frequencies of $D_x(\omega)$ are compared for a typical range of the above parameters in Fig. 4. According to Fig. 3, $k_x < 0$ for the whole study range, and therefore the system is stable (grey area) when $D_{r,\,vsc}(\omega_x) < D_{r,\,grid}(\omega_x)$ (24). The sensitivity analysis results are verified with the root locus plot of the poorly damped poles in Fig. 5. Note that the poles go from the RHS to the LHS of the Nyquist plot for the parameter values labelled in the plot, meaning that the system becomes stable. These values match with the values obtained in Fig. 4. According to the above study, Fig. 6 shows five cases where the stability is achieved by increasing or decreasing the values of the previous parameters up to $SCR = 2.25$ (Case #1), $\omega_f = 5\omega_{f,\,ref}$ (Case #2), $\omega_c = 2\omega_{c,\,ref}$ (Case #3), $\omega_{dc} = 3\omega_{dc,\,ref}$ (Case #4) and $\omega_p = 0.2\omega_{p,\,ref}$ (Case #5). The impedance matrix determinant-based stability criterion (15) predicts the stability of the above cases because, in the neighborhood of the poorly damped poles, $k_x < 0$ and $D_r(\omega_x) < 0$ at the zero-crossing frequencies of $D_x(\omega)$. The alternative approach in Section 4 also confirms the stability because $D_{r\,vsc}(\omega_x) < D_{r\,grid}(\omega_x) = -X_{g1}^2$ (24) at the zero-crossing frequencies of $D_x(\omega)$. The GNC verifies the results on instability because the curves of the eigenvalues λ_1 and λ_2 (8) do not encircle the −1 point in any case. Note that, unlike impedance matrix determinant-based stability criterion and the GNC, the proposed approach shows that the stability is achieved because the VSC term $D_{r,\,vsc}(\omega_x)$ compensates the weak grid term $D_{r,\,grid}(\omega_x)$. PSCAD/EMTDC time-domain simulations validate the above results. It is observed that the system becomes unstable when the WTG output active power P_{WTG} is raised to 0.1 pu (reference case) at 0.1 s and it goes out of instability if the parameters *SCR*, ω_f, ω_c, ω_{dc} and ω_p are stepped to 2.25 (Case #1), $5\omega_{f,\,ref}$ (Case #2), $2\omega_{c,\,ref}$ (Case #3), $3\omega_{dc,\,ref}$ (Case #4) and $0.2\omega_{p,\,ref}$ at 0.5 s.

5.3. Understanding the influence of parameters on stability

The influence of the different system parameters on SSOs cannot be clearly analyzed with the traditional frequency domain stability methods [3], [6], [9], [20] – [22] and the impedance matrix determinant-based stability criterion [3]. On the other way, the alternative approach in Section 4 allows clearly analyzing the contribution of VSCs and grid to stability because it evaluates SSOs from the comparison between the VSC ($D_{r,\,vsc}$ or $D_{x,\,vsc}$) and grid ($D_{r,\,grid}$ or $D_{x,\,grid}$) terms. This provides a criterion for understanding the influence of grid and VSCs on stability.

Analyzing the alternative approach plots in Fig. 3 and Fig. 6, the following conclusions can be obtained:

- Reference case: The grid term $D_{r,\,grid}$ is smaller than the VSC term $D_{r,\,vsc}$, (24) due to the high value of the grid reactances (i.e., the low value of the SCR) and the system is unstable. This means that SSOs caused by any electrical event are increased by the high reactance value of weak grids and VSC control is not able to mitigate these oscillations becoming the system unstable.
- Influence of electrical parameters (Case #1): Increase of short-circuit ratio (26) by reducing the transmission line reactance x_Σ or increasing the number N of WTGs mainly reduces the off diagonal term X_{g1} in (27) at subsynchornous frequencies. This may lead the grid term $D_{r,\,grid}$ (24) above VSC term $D_{r,\,vsc}$ at resonance frequency and system turns stable (i.e., VSC control can mitigate possible increase of SSOs due to grid

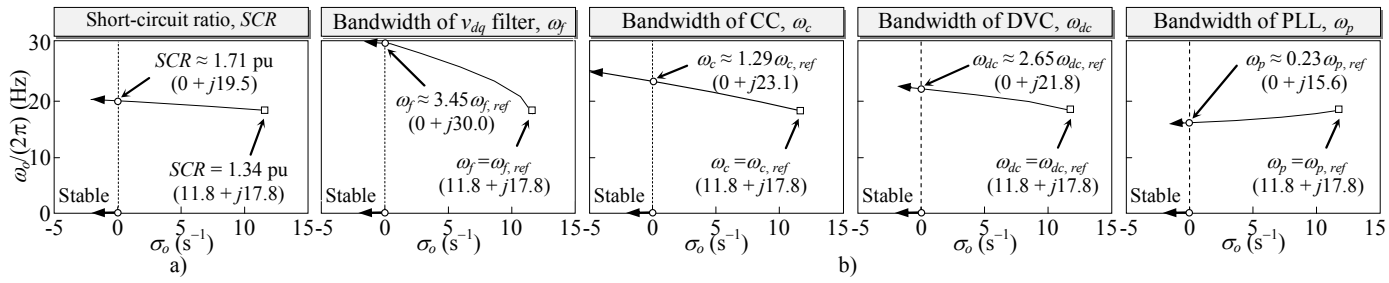

Fig. 5. *Influence of system parameters on root locus of the poorly damped poles (conjugate poles are not plotted for clarity)*
(a) *SCR*, **(b)** ω_f, ω_c, ω_{dc} and ω_p.

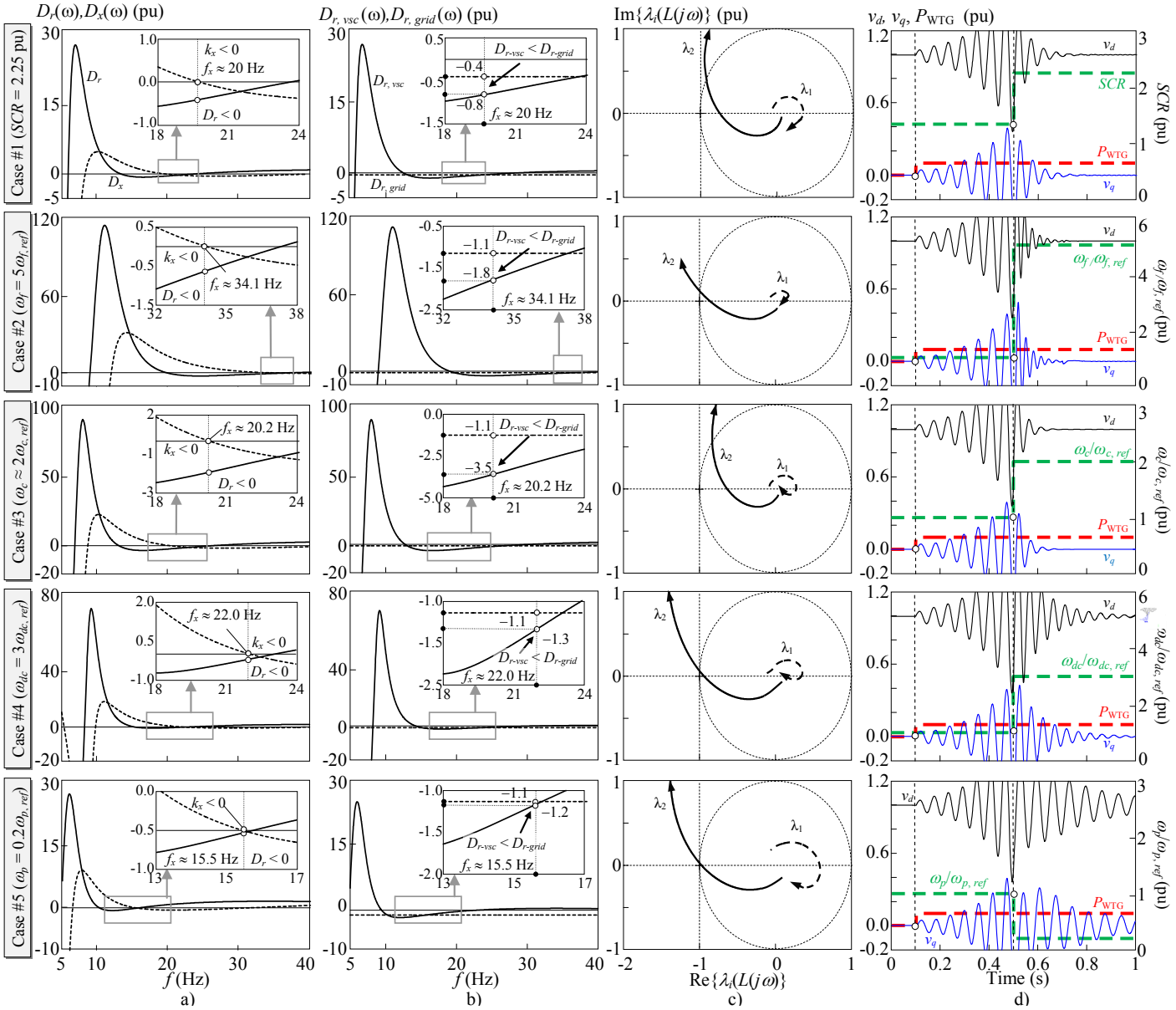

Fig. 6. *Influence of system parameters on stability*
(a) Impedance matrix determinant-based stability criterion, **(b)** Alternative approach in the paper, **(c)** Generalized Nyquist criterion, **(d)** PSCAD/EMTDC time-domain simulations.

reactances). Large values of short-circuit ratio could also be obtained by reducing the number of online WTGs N, which increases VSC impedances in (27). In this situation, the system may also turn stable if $D_{r,\,vsc}$ becomes smaller than $D_{r,\,grid}$.

- Influence of VSC control parameters (Case #2, #3, #4 and #5): Control parameters should lead the VSC term $D_{r,\,vsc}$ below the grid term $D_{r,\,grid}$ (24) by changing VSC impedances in (27) in order to obtain system stability. This would allow that VSC control could mitigate possible SSOs caused by high reactance values of weak grids:

  - Case #2: High bandwidths of the feed-forward voltage low-pass filter, ω_f, improve the VSC voltage disturbance rejection capability and instability may be avoided.
  - Case #3 and #4: Fast VSC inner and outer controls (i.e., high bandwidths of inner and outer control loops, ω_c and ω_{dc}) improve control dynamics to SSOs and it has positive impact on instability mitigation. This can also be achieved by increasing the proportional gains of the CC and DVC ($k_p = \omega_c L$ and $k_{p\text{-}dc} = \omega_{dc} C$, respectively). These results are different than those in [22] because the present study considers the contribution of the grid and VSC on system stability while [22] only analyzes the damping contribution of the VSC.
  - Case #5: Low bandwidths of the PLL loop, ω_p, allow filtering SSOs and improving system stability. This can also be achieved by reducing the proportional gain of the PLL, $k_{p\text{–}PLL} = \omega_p / v_0$. This recommendation was also proposed in [22] but the presented approach shows the contribution that the grid and VSC have on stability.

It is worth noting that the reduction of term $D_{r,\,vsc}$ in (24) can be obtained by other procedures than increasing the damping of VSC impedance as it is usually recommended in the literature [8], [20] – [22]. Fig. 7 illustrates that the VSC

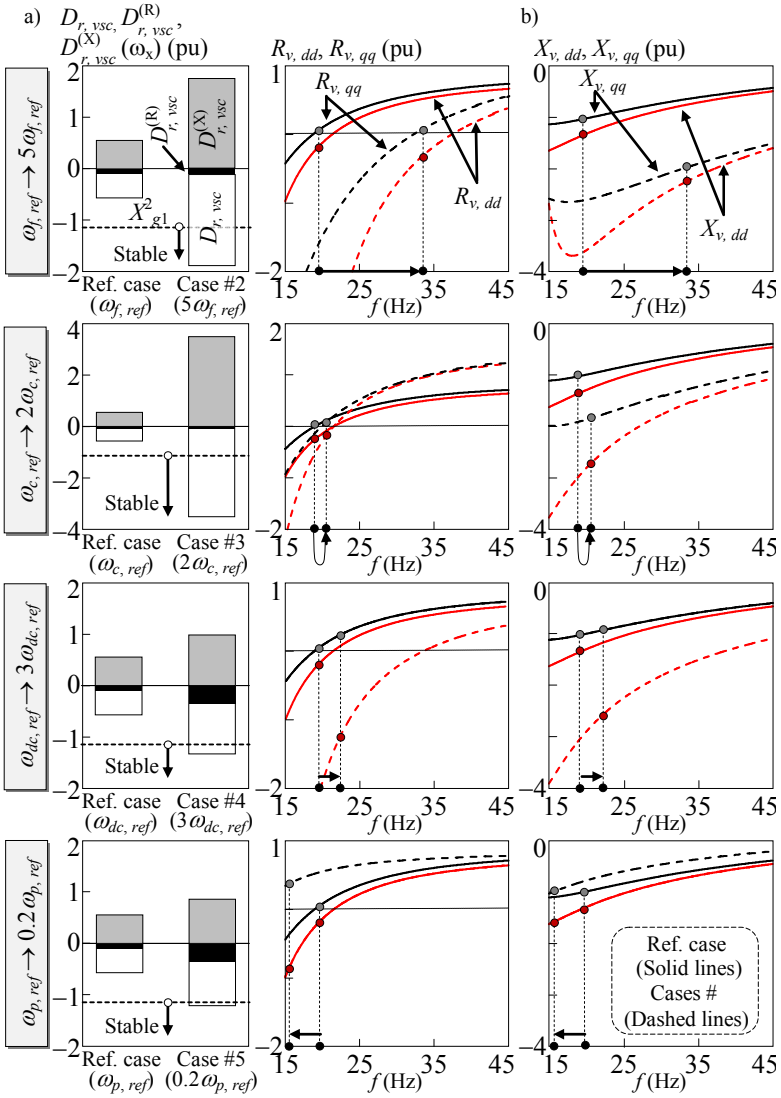

Fig. 7. *Understanding the influence of VSC control parameters on stability*
(a) $D_{r,\,vsc}$ terms, **(b)** VSC resistance and reactance values.

control recommendations for improving system stability should not be necessarily aimed to increase the damping of the VSC impedance. Fig. 7(a) compares the terms $D_{r,\,grid} = -X^2_g$ and $D_{r,\,vsc}$ in the reference case and the Cases #2 to #5, and also shows the contribution of the terms $D^{(R)}{}_{r,\,vsc}$ and $D^{(X)}{}_{r,\,vsc}$ to $D_{r,\,vsc}$ (24), i.e.,

$$D_{r,vsc}(\omega_x) = \underbrace{R_{v,dd}R_{v,qq}}_{D^{(R)}_{r,vsc}(\omega_x)} - \underbrace{(X_{v,dd}+X_g)(X_{v,qq}+X_g)}_{D^{(X)}_{r,vsc}(\omega_x)}. \qquad (28)$$

It can be observed that the feed-forward voltage low-pass filter (Case #2) and the CC (Case #3) improve stability by mainly increasing the term $D^{(X)}{}_{r,\,vsc}$ (i.e., the VSC equivalent reactances $X_{v,\,dd}$ and $X_{v,\,qq}$ in Fig. 7(b)) while the DVC (Case #4) and PLL loop (Case #5) improve stability by varying both terms $D^{(R)}{}_{r,\,vsc}$ and $D^{(X)}{}_{r,\,vsc}$. The DVC modifies only the *d*-component of the VSC equivalent impedance while the PLL loop modifies only the *q*-component in Fig. 7(b).

6. Conclusions

This paper studies the influence that electrical and control parameters have on SSOs in AC grids with WTG VSCs. This is a new phenomenon different from the classical voltage instability. The paper contributes with a new approach for analyzing the contribution that grid and VSC have on stability. This approach analyzes two terms of the system impedance determinant that represent the contribution that the VSC and the grid have on the system stability. This allows understanding the influence that electrical system and control parameters have on stability. It is concluded that changes on VSC or grid parameters may be used to independently modify these two terms in order to achieve stability. It is observed that stability margins do not only depend on the damping of the system (i.e., on the resistances) but also depends on the system reactances. It is verified that the risk of SSOs may be mitigated reducing the value of the grid reactance by decreasing the number of transformers or by connecting new transmission lines [1], [3], because this could reduce the grid term of the determinant which directly depends on the grid reactance. Also, the paper presents the following recommendations about the SSOs mitigation from the VSC control:

- Large bandwidth of the feed-forward voltage filter improves control dynamics against SSOs.

- Large bandwidths of the CC and DVC also improve control dynamics against SSOs.
- PLL loop bandwidths should not be unnecessarily large in weak AC grids to avoid SSOs.

It is observed that similar recommendations are presented in the literature for improving voltage stability although it is a different phenomenon than SSOs.

The new approach presented in the paper and the analysys and recommendations on SSOs may be used to design power system stabilizers.

7. Acknowledgments

This work was supported in part by the Ministerio de Ciencia, Innovación y Universidades (grant RTI2018-095720-B-C33); the Ministerio de Economía, Industria y Competitividad and the EU FEDER Funds (grant DPI2017-84503-R). L. Monjo would also like to thank Universitat Jaume I for their support to this work under the grant E-2017-47.

8. References

[1] Sun, J., Li, M., Zhang, Z., Xu, T., He, J., Wang, H., Li, G.: 'Renewable energy transmission by HVDC across the continent: System challenges and opportunities', CSEE Journal of Power and Energy Systems, 2017, 3, (4), pp. 353–364.

[2] Koraki, D., Strunz, K.: 'Wind and solar power integration in electricity markets and distribution networks through service-center virtual power plants', IEEE Trans. on Power Syst., 2018, 33, (1), pp.473-485.

[3] Liu, H., Xie, X., He, J., Xu, T., Yu, Z., Wang, C., Zhang, C.: 'Subsynchronous interaction between direc-drive PMSG based wind farms and weak AC networks', IEEE Trans. on Power Syst., 2017, 32, (6), pp. 4708–4720.

[4] Mitra, A., Chatterjee, D.: 'Active power control of DFIG-based wind farm for improvement of transient stability of power systems', IEEE Trans. on Power Syst., 2016, 31, (1), pp. 82–93.

[5] Variani, M. H., Tomsovic, K.: 'Two-level control of doubly fed induction generator using flatness-based approach', IEEE Trans. on Power Syst., 2016, 31, (1), pp. 518–525.

[6] Liu, H. K., Xie, X., Zhang, C., Li, Y., Liu, H., Hu, Y.: 'Quantitative SSR analysis of series-compensated DFIG-based wind farms using aggregated RLC circuit model', IEEE Trans. on Power Syst., 2017, 32, (1), pp. 474-483.

[7] Wang, Y., Meng, J., Zhang, X., Xu, L.: 'Control of PMSG-based wind turbines for system inertial response and power oscillation damping', IEEE Trans. Sustain. Energy, 2015, 6, (2), pp. 565–574.

[8] Harnefors, L., Wang, X., Yepes, A. G., Blaabjerg, F.: 'Passivity-based stability assessment of grid-connected VSCs – An overview', IEEE Journal of Emerging and Selected Topics in Power Electronics, 2016, 4, (1), pp. 116–125.

[9] Stamatiou, G., Bongiorno, M.: 'Stability Analysis of Two-Terminal VSC-HVDC Systems using Net-Damping Criterion', IEEE Trans. on Power Delivery, 2016, 31, (4), pp. 1748-1756.

[10] Freijedo, F. D., Chaudhary, S. K., Teodorescu, R., Guerrero, J. M., Bak, C. L., Kocewiak, L. H., Jensen, C. F.: 'Harmonic resonances in wind power plants: modeling, analysis and active mitigation methods', Proc. of the IEEE PowerTech Eindhoven, June-July 2015, pp. 1-6.

[11] Aeberhard, M., Meyer, M., Courtois, C.: 'The new standard EN 50388-2, Part 2—Stability and harmonics', Elektrische Bahnen, 2014, 12, (1), pp. 28–35.

[12] Liu, H., Xie, X., Gao, X., Liu, H., Li, Y.: 'Stability Analysis of SSR in Multiple Wind Farms Connected to Series-Compensated Systems using Impedance Network Model', IEEE Trans. on Power Syst., 2018, 33, (3), pp.3118-3128.

[13] Liu, H., Xie, X., Liu, W.: 'An Oscillatory Stability Criterion based on the Unified dq-Frame Impedance Network Model for Power Systems with High-Penetration Renewables', IEEE Trans. on Power Syst., 2018, 33, (3), pp. 3472-3485.

[14] Fan, L., Miao, Z.: 'Mitigating SSR using DFIG-based wind generation', IEEE Trans. Sustain. Energy, 2012, 3, (3), pp. 349-358.

[15] Lu, J., Nehrir, M. H., Pierre, D. A.: 'A fuzzy logic-based self tuning power system stabilizer optimized with a genetic algorithm', Electric Power Systems Research, 2001, 60, pp. 77-83.

[16] Sambariya, D. K.: 'Power system stabilizer design using compressed rule base of fuzzy logic controller', Journal of Electrical and Electronic Engineering, 2015, 3, (3), pp. 52-64.

[17] Shayanfar, H., Shayeghi, H., Abedinia, O., Jalili, A.: 'Design Rule-Base of Fuzzy Controller in Multimachine Power System Stabilizer Using Genetic Algorithm', Proc. of the IEEE PowerTech Eindhoven, June-July 2015, pp. 1-6.

[18] Preece, R., Milanovic, J. V., Almutairi, A. M., Marjanovic, O.: 'Damping of inter-area oscillations in mixed AC/DC networks using WAMS based supplementary controller', IEEE Trans. on Power Syst., 2013, 28, (2), pp. 1160-1169.

[19] Zhang, C., Cai, X., Li, Z., Rygg, A., Molinas, M.: 'Properties and physical interpretation of the dynamic interactions between voltage source converters and grid: electrical oscillation and its stability control', IET Power Electronics, 2017, 10, (8), pp. 894-902.

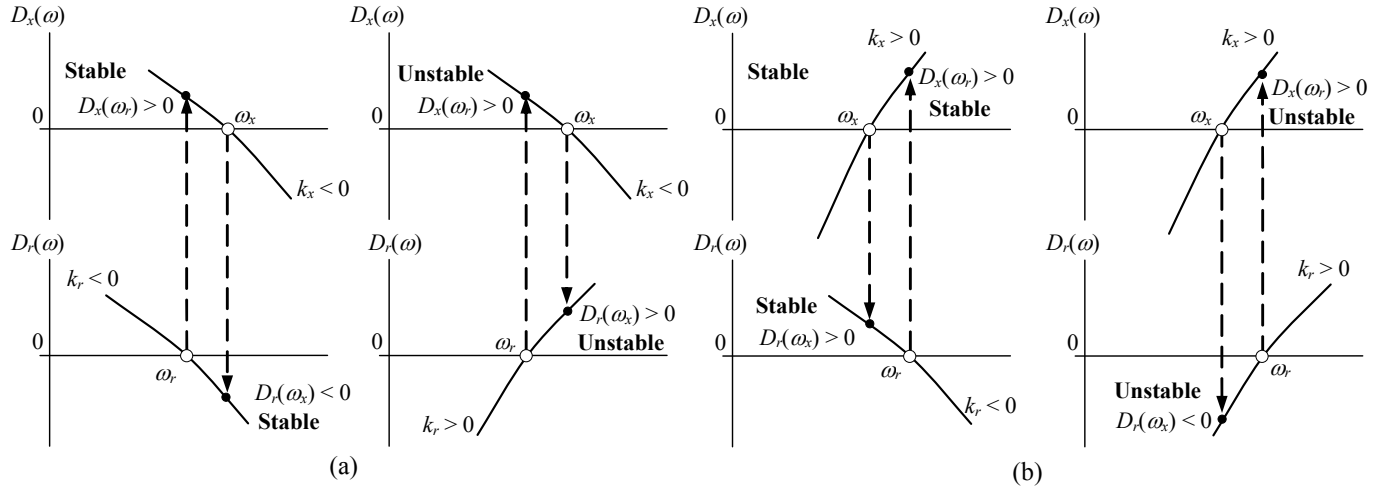

Fig. 8. *Study of the impedance matrix determinant-based stability criterion*
(a) $\omega_x > \omega_r$, **(b)** $\omega_x < \omega_r$.

[20] Alawasa, K. M., Mohamed, Y. A. I., Xu, W.: 'Modeling, analysis, and suppression of the impact of full-scale wind-power converters on subsynchronous damping', IEEE Syst. J., 2013, 7, (4), pp. 700–712.

[21] Alawasa, K. M., Mohamed, Y. A. I., Xu, W.: 'Active mitigation of subsynchronous interactions between PWM voltage-source converters and power networks', IEEE Trans. Power Electron., 2014, 29, (1), pp. 121–134.

[22] Harnefors, L., Bongiorno, M., Lundberg, S.: 'Input-admittance calculation and shaping for controlled voltage-source converters', IEEE Trans. on Industrial Electronics, 2007, 54, (6), pp. 3323-3334.

[23] Larsen, E. V.: 'Wind generators and series-compensated AC transmission lines," in Proc. 2012 IEEE Power Energy Soc. Transm. Distrib. Conf. Expo., 2012, pp. 1–4.

[24] Ma, H. T., Brogan, P. B., Jensen, K. H., Nelson, R. J.: 'Sub-synchronous control interaction studies between full-converter wind turbines and seriescompensated AC transmission lines', in Proc. 2012 IEEE Power Energy Soc. General Meeting, 2012, pp. 1–5.

[25] Harnefors, L.: 'Modeling of Three-Phase Dynamic Systems Using Complex Transfer Functions and Transfer Matrices', IEEE Transactions on Industrial Electronics, 2007, 54, (4), pp. 2239-2248.

[26] Kundur, P.: 'Power System Stability and Control'.: McGraw-Hill Education.

[27] Wang, X., Harnefors, L., Blaabjerg, F.: 'Unified impedance model of grid-connected voltage-source converters', IEEE Transactions on Industrial Electronics, 2018, 33, (2), pp. 1775-1787.

9. Appendix: Impedance matrix determinant-based stability criterion

Criteria (15) and (18) for assessing system stability are analyzed graphically by comparing all possible combinations of the impedance matrix determinant-based stability criterion. An example of these combinations is shown in Fig. 8. The curves in Fig. 8 represent the $D_r(\omega)$ and $D_x(\omega)$ plots around the real and imaginary part zero-crossing frequencies of the poorly damped zeros. It is concluded that both criteria lead to the same prediction. Although the other combinations of the impedance matrix determinant-based stability criterion are not shown for space reasons, the previous conclusion is also true for all of them.